Chemistry
Europe
European Chemical
Societies Publishing

The gas diffusion electrode setup as a testing platform for evaluating fuel cell catalysts: A comparative RDE-GDE study

Sven Nösberger[1] | **Jia Du**[1] | **Jonathan Quinson**[2] | **Etienne Berner**[1] |
Alessandro Zana[1] | **Gustav K.H. Wiberg**[1] | **Matthias Arenz**[1]

[1]Department of Chemistry, Biochemistry, and Pharmaceutical Sciences, University of Bern, Bern, Switzerland

[2]Department of Chemistry, University of Copenhagen, Copenhagen Ø, Denmark

Correspondence
Matthias Arenz, Department of Chemistry, Biochemistry and Pharmaceutical Sciences, University of Bern, Freiestrasse 3, 3012 Bern, Switzerland.
Email: matthias.arenz@unibe.ch

Sven Nösberger and Jia Du are equally contributing first authors.

Abstract

Gas diffusion electrode (GDE) setups have been recently introduced as a new experimental approach to test the performance of fuel cell catalysts under high mass transport conditions, while maintaining the simplicity of rotating disk electrode (RDE) setups. In contrast to experimental RDE protocols, for investigations using GDE setups only few systematic studies have been performed. In literature, different GDE arrangements were demonstrated, for example, with and without an incorporated proton exchange membrane. Herein, we chose a membrane-GDE approach for a comparative RDE–GDE study, where we investigate several commercial standard Pt/C fuel cell catalysts with respect to the oxygen reduction reaction (ORR). Our results demonstrate both the challenges and the strengths of the new fuel cell catalyst testing platform. We highlight the analysis and the optimization of catalyst film parameters. That is, instead of focusing on the intrinsic catalyst ORR activities that are typically derived in RDE investigations, we focus on parameters, such as the catalyst ink recipe, which can be optimized for an individual catalyst in a much simpler manner as compared to the elaborative membrane electrode assembly (MEA) testing. In particular, it is demonstrated that ∼50% improvement in ORR performance can be reached for a particular Pt/C catalyst by changing the Nafion content in the catalyst layer. The study therefore stresses the feasibility of the GDE approach used as an intermediate "testing step" between RDE and MEA tests when developing new fuel cell catalysts.

KEYWORDS
gas diffusion electrode (GDE) setups, fuel cell catalysts, oxygen reduction reaction (ORR), rotating disk electrode (RDE) setups

1 | INTRODUCTION

Despite the substantial advancements of fuel cells in the last decade, their cost and the lack of a hydrogen infrastructure are still inhibiting factors for mass commercialization. Concerning fuel cell catalysts, the amount of Pt (precious metal) used and its resistance against degradation are major factors that still need further improvement.[1–5] To reduce the costs, the catalyst layers need to be improved in a way that they provide maximal power by minimal Pt (precious metal) content. Additional challenges are the scarcity of the active catalyst materials and the limited conversion efficiency (as compared to battery storage).[6] Developing new and improved oxygen reduction reaction (ORR) catalysts with lower precious metal content that achieve higher power densities is therefore crucial. One major challenge thereby is the implementation of new catalysts established in fundamental research to applications in fuel cells. Despite the fact that many promising catalysts meet performance targets identified in rotating disk electrode (RDE) measurements, there are few examples of successful implementation to membrane electrode assembly (MEA) testing.[7]

In fundamental research, most fuel cell catalysts are investigated with a RDE setup.[8] However, due to the limited mass transport, inherent to RDE setups, the potential ranges at which the kinetics of an ORR catalyst can be investigated is narrow. In addition, different catalyst loadings and testing parameters are used for RDE measurements compared to MEAs, that is, the typical catalyst loading for RDE is 5–20 $\mu g_{Pt}/cm^2$, while for MEAs it is 100–500 $\mu g_{Pt}/cm^2$, which leads to different thicknesses in catalyst layers.[8–10] In RDE measurements, the catalyst layer may contain Nafion (or similar proton conducting polymer) binder. However, due to the liquid electrolyte, this is not required for proton transport. By comparison, Nafion is an essential component for catalyst layers in MEAs. Furthermore, RDE testing protocols are performed potentiodynamically, while MEAs testing is carried out under potentiostatic or galvanostatic conditions.[9] All these differences limit the transferability of results gained with an RDE setup toward an application in fuel cells. There is a lack of evidence that all high-performing fuel cell catalysts measured with the RDE setup can unfold their full potential in MEAs.[7,11,12]

To facilitate the full exploitation of results and knowledge obtained in fundamental research, new measurement setups with increased mass transport properties have been introduced.[7,13–19] These setups allow to apply more realistic conditions in the catalyst testing and at the same time should be widely applicable in standard research laboratories. The GDE approach fulfils these criteria.[18,20–23] Most importantly, mass transport limitations which are inherent to RDE measurements, can be avoided in the GDE approach by distributing the reactant, for example, oxygen gas, directly through a gas diffusion layer (GDL). In the article, the used membrane-based GDE setup, no direct contact between catalyst layer and liquid electrolyte exists. A polymer electrolyte membrane separates the catalyst layer, which in the current study contains a fixed Pt loading of 208 $\mu g_{Pt}/cm^2$, and the electrolyte. A major challenge for the GDE approach is to develop and standardize procedures for catalyst testing.[23] Therefore, it is of interest to systematically compare the inherent performance of Pt/C catalysts as determined by RDE measurements with their performance as catalyst film in membrane-GDE measurements. In the presented study, we thus, compare the ORR performance of six different commercial Pt/C catalysts in a GDE setup and use RDE measurements as benchmark for their *intrinsic* ORR activity. The aim is to investigate which factors are essential to transfer the *intrinsic* ORR activity of Pt/C catalysts to catalyst layers that eventually will be used in MEAs. The experimental protocol (e.g., catalyst ink composition, coating methods, and measurement procedures) in the RDE measurements utilizes previous insights on establishing *intrinsic* activities, whereas the GDE protocol is oriented toward MEA testing. However, both experimental protocols fulfil the respective testing criteria to reach the fundamental and applied research standard, as closely as possible.[8,24–26] With this study, it is demonstrated that a GDE approach allows a straight-forward optimization of a given catalyst film under conditions relevant for applications. On the other hand, GDE testing using standardized ink recipes might not uncover the full potential of a respective catalyst.

2 | MATERIALS AND METHODS

2.1 | Small angle X-ray scattering (SAXS)

Small angle X-ray scattering (SAXS) measurements were conducted using a SAXSLab instrument as previously described[22] and are detailed in Supporting information. The SAXS data were fitted assuming a power law and polydisperse spheres. The background corrected scattering data were fitted using a power law to take into account the behavior at low q value and a model of polydisperse spheres, described by a volume-weighted log-normal distribution. Some data were best fitted by adding a second model of polydisperse spheres also described by a volume-weighted log-normal distribution. The scattering data and related fits are reported in Supporting information Figure S1 and the values obtained for the fitting parameters are reported in Supporting information Table S1.

2.2 | Transmission electron microscopy (TEM) and scanning electron microscopy with energy dispersive X-ray spectroscopy (SEM-EDS)

A Jeol 2100 transmission electron microscope (TEM) operated at 200 kV was used for the TEM analysis. The samples were prepared by suspending the commercial catalyst powders in ethanol and then dropping the sample suspension onto carbon-coated copper TEM grids (copper or nickel grids, Quantifoil). Micrographs were recorded at three different magnifications at least, and in at least three randomly selected areas. At least 200 nanoparticle diameters were evaluated using the software ImageJ to evaluate the size distribution.

The SEM-EDS cross-section measurements were performed as described earlier[21] using a Zeiss GeminiSEM 450 with SmartSEM 6.05 software and EDS Photodetector Ultim max 65 from Oxford Instruments using AZTec 4.2 software. As scan parameters for the EDS maps, a WD (working distance) between 8.4 and 8.8 mm, accelerating voltage of 15 kV and a probe current of 200 pA were used.

2.3 | Electrochemical characterization

2.3.1 | Catalyst ink and film formation for the RDE measurements

The inks for the RDE measurements were prepared from the respective dried catalyst powder and dispersed in a mixture of Milli-Q water and isopropanol (V_{water}: V_{IPA} = 3: 1). To the ink, 1.6 μL/mL 1 M KOH (aq) was added and then homogenized in a sonicator bath for 10 min. The resulting homogeneous catalyst ink had a total Pt concentration of 0.218 g_{Pt}/L.

Thin catalysts films were prepared by pipetting 9 μL (0.218 g_{Pt}/L) of each catalyst ink onto a newly polished glassy carbon (GC) disc. The disk was then dried under Ar gas stream humidified with IPA and H_2O, the disc was kept stationary in the drying step. The resulting films had a Pt loading of 10 μg/cm^2 and were dried at ambient atmosphere for further electrochemical measurements.

2.3.2 | Catalyst ink and film preparation for the GDE measurements

Catalysts inks were prepared from different dried catalyst powders and dispersed in a mixture of Milli-Q water and isopropanol (mixture volume ratio of 3:1). To disperse the powder, the mixture was sonicated for 5 min at room tem-perature. Subsequently, Nafion solution was added so that the ink contained a mass C:Nafion ratio of 1. The ink was sonicated again for 5 min. The final inks had a Pt concentration of 0.5 mg/mL for all catalysts.

The catalyst films were produced by a vacuum filtration of the catalyst ink onto GDL. To conduct the vacuum filtration, the ink was first diluted by Milli-Q water to a Pt concentration of 0.05 mg/mL (mixture volume ratio 1:3). The ink was then added to a vacuum apparatus and filtrated through an MPL-coated GDL (Freudenberg H23C8). The resulting catalyst films (∅ = 4 cm) were stored in petri dishes. From this film-coated GDL, a disk (∅ = 3 mm) was extruded and used as GDE. All investigated GDEs prepared from the commercially available Pt/C catalysts had a Pt loading of 208 ug_{Pt}/cm^2 on the GDL.

2.3.3 | Rotating disk electrode (RDE) measurements

All RDE electrochemical measurements were performed at room temperature with a computer controlled potentiostat (ECi 200, Nordic Electrochemistry ApS) and a glass cell equipped with three electrodes as previously reported.[26–28] The working electrode (WE) was a GC disk (5 mm in diameter) embedded into a Teflon tip.

A Pt wire served as counter electrode (CE) and a reversible hydrogen electrode (RHE) served as a reference electrode. An aqueous 0.1 M perchloric acid electrolyte was used, which was saturated with argon prior to the start of the electrochemical measurements. The solution resistance was measured with a superposed AC signal (5 mV, 5 kHz) and was compensated down to 2 Ω.

The analytical procedure to electrochemically analyze the Pt/C catalyst layers was repeated for all six investigated Pt/C catalysts and included the following steps: Surface cleaning, Ar background, ORR activity, and CO stripping to determine Pt active surface area. The Pt catalyst surface was cleaned under an argon atmosphere by cycling the potential between 0.05 V_{RHE} and 1.20 V_{RHE} for three cycles to remove the possible organic residue on the catalyst film. Thereafter, the upper potential was reduced to 1.10 V_{RHE} and the cycling was continued until reaching a stable cyclic voltammogram (CV) (∼50 cycles in total). The scan rate was 0.50 V/s. The initial higher potential limit served to reduce the total number of potential sweeps. Afterwards, an Ar background was measured in a potential range between 0.05 V_{RHE} and 1.10 V_{RHE} with a scan rate of 0.05 V/s in Ar saturated electrolyte. Prior to the ORR performance measurements, the electrolyte was purged with O_2 for 10 min. During the ORR activity measurement, the potential window and the scan rate were the same as that

4   **Electrochemical Science Advances**   RESEARCH ARTICLE
doi.org/10.1002/elsa.202100190

Chemistry
Europe
European Chemical
Societies Publishing

applied for Ar background measurements, while the RDE had a rotation speed of 1600 rpm.

To determine the electrochemical active surface area (ECSA) of the investigated catalysts, the oxidation charge obtained from a CO monolayer stripping experiments was analyzed. In brief, the electrode was held at 0.05 V_{RHE} in CO saturated electrolyte for 2 min. Subsequently, the electrolyte was saturated with Ar (~10 min) to purge the electrolyte from CO. The potential was swept from 0.05 to 1.10 V_{RHE} with a scan rate of 50 mV/s to oxidize the adsorbed CO monolayer to CO_2. The ECSA was then calculated from the ration of resulting oxidative charge (Q_{CO}), after background subtraction, and the oxidation charge of a monolayer, 400 $\mu C/cm_{Pt}^2$, and finally normalized to the mass of the Pt (m_{Pt}).[29]

$$ECSA = \frac{Q_{CO}}{400 \mu C \, cm_{Pt}^{-2}} \frac{1}{mPt}.$$

The ORR data were analysed from the background corrected polarization curves. The background polarization curves were recorded in Ar-purged electrolyte. The ORR activity was then evaluated at 0.90 V_{RHE} from positive going scans. The mass activity (MA) was obtained by normalizing the activity by the Pt mass. The specific activity (SA) was obtained by normalizing the measured current density (mA/cm_{Geo}^2) to the ECSA.

2.3.4 | Measurements in the gas diffusion electrode setup

The GDE-setup was assembled as follows:[13] A 3 mm disc was punched out of the catalyst film covered by GDL. The catalyst containing disc was placed into an MPL-coated GDL disc (Ø = 2 cm, Freudenberg H23C8) which had a 3 mm hole in the middle. A Nafion membrane was placed on top (Nafion 117, thickness 183um). With a tablet press (pressure range: 0–15T), the whole stack was pressed together at a pressure of two tonnes and a duration of 10 min. Afterwards, a GDL (Freudenberg H23) was placed into the gas flow field of the lower cell body, followed by the stack containing the GDE and the Nafion membrane. Finally, the upper cell body was placed on top of the Nafion membrane. The two body parts were held in place by a clamp. The compartments of the upper cell body were filled with 15 mL of 4 M perchloric acid. Finally, an RHE RE and the CE (Pt wire) were put into the electrolyte.

All electrochemical measurements were performed at 30°C with a computer controlled potentiostat (ECi 240, Nordic Electrochemistry ApS) and a GDE-setup as reported.[13] The analytical procedure to electrochemically analyse the Pt/C catalyst layers was the same for all

six investigated Pt/C catalysts and included the following steps: First, the GDE was purged from the backside (through the GDL) with argon gas. Doing so, the catalyst was cleaned by potential cycles between 0.05 and 1.10 V_{RHE} at a scan rate of 0.2 V/s until a stable CV could be observed (~50 cycles). Afterwards, a CO stripping measurement was performed followed by electrochemical impedance spectroscopy (EIS) and ORR-activity measurements. To conclude the investigations, a second CO stripping measurement was performed. Throughout the entire experiment, a bubbler was used to humidify the gas and the membrane. During the whole measurement, the solution resistance was measured by superimposing an AC signal of 5 kHz and an amplitude of 5 mV.

CO stripping measurements were conducted to determine the ECSA. In essence, the catalyst layer got covered by CO gas which adsorbed onto the Pt surface. Afterwards, the catalyst was purged with Ar to remove the excess of CO. As a next step, a CV was recorded (scan rate: 50 mV/s), which records the oxidative current originating from the oxidation of CO to CO_2. Finally, multiple CVs under Ar atmosphere were conducted until the Ar background was regained. The value of the ECSA was then obtained, as described in "Section 2.3.3".

Prior to the ORR activity measurements, oxygen was flowed through the pipes for 10 min. For the last 5 min, a potential of 0.80 V_{RHE} was applied. This ensured that all gas lines were fully filled with oxygen and that the catalyst layer was equally wet over the entire surface. The ORR-activity measurements were conducted in potential control mode with a potential range between 1.00 V_{RHE} and 0.10 V_{RHE}. The potential was preset to 1.00 V_{RHE} and then lowered in steps of 25 mV until 0.10 V_{RHE} are reached. At every step, the potential was held constant for 1 min to reach steady-state conditions. For analysis, the measured current was averaged over the last 10 s. The online solution resistance was determined from the superimposed AC signal (5 kHz, 5 mV). All ORR activity measurements were postcorrected for the potential errors introduced by the solution resistance using this online measurement, see Supporting information Figure S2 for example. The EIS measurements served to back up the online correction in case of failure or uncertainties.

3 | RESULTS AND DISCUSSION

We start with the physical characterization of the investigated Pt/C fuel cell catalysts. All examined catalysts are commercially available and can serve as benchmarks in studies investigating new, home-made fuel cell catalysts. Their Pt to C ratio (Pt loading), as indicated by the supplier, ranges from roughly 20 wt.% up to 70 wt.%. In Figure 1,
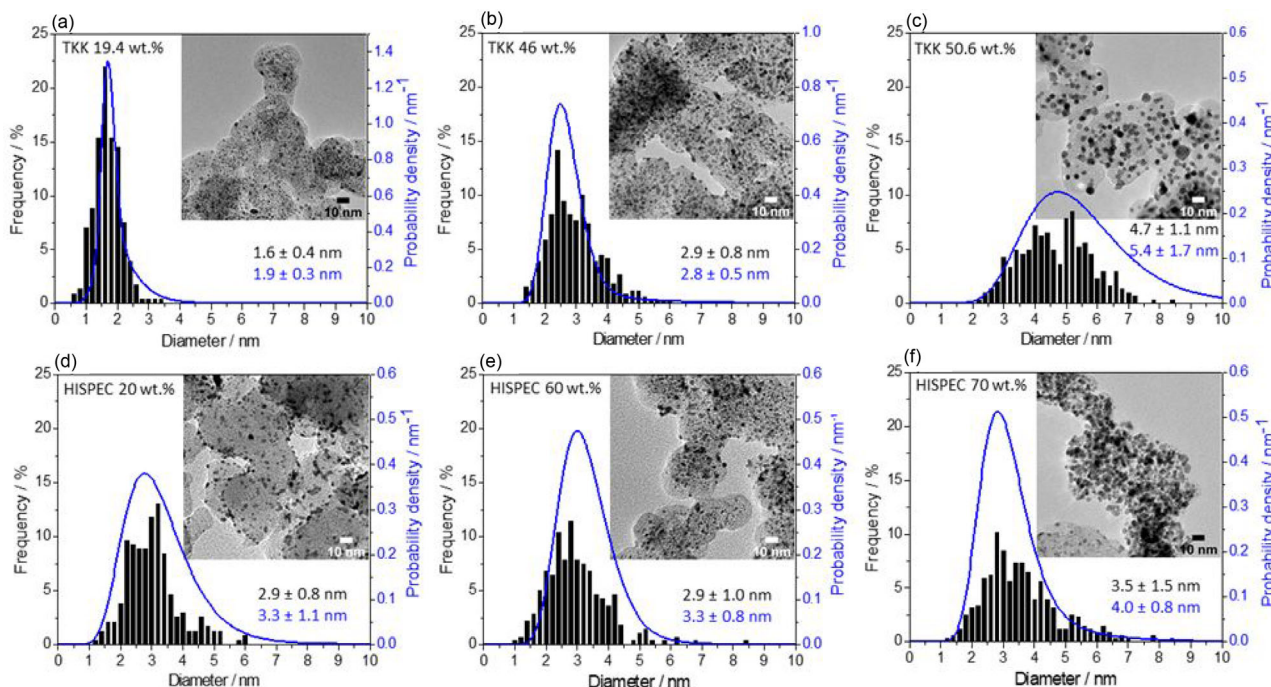
5 **Electrochemical Science Advances**

RESEARCH ARTICLE
doi.org/10.1002/elsa.202100190

Chemistry Europe
European Chemical
Societies Publishing

FIGURE 1 Pt particle size distribution of the investigated commercial Pt/C determined from TEM micrographs (at least 200 particles were counted) and probability density function derived from the SAXS analysis. The insets display representative TEM micrographs of each commercial Pt/C catalyst. The average particle size with the font in black is determined from TEM measurements while the blue font indicates the average particle size determined from the SAXS measurements. The Pt-to-C ratio (Pt loading) of each Pt/C catalyst is indicated in the upper left corner

we present representative TEM micrographs to demonstrate the physical characteristics of each Pt/C catalyst. In addition, size histograms and average particle sizes derived from a TEM analysis as well as probability density functions derived from fitting the SAXS data are shown. As Figure 1 shows, within the accuracy (error) of the measurements, both methods lead to the same average particle size. However, with a closer look at the size retrieved, the average Pt particle size determined from TEM is slightly smaller (except for TKK 46 wt.% Pt/C) in comparison to the values derived from the SAXS analysis. This difference can be explained by the fact that the particle size distributions are based on different analyses that are sensitive to different sizes in different ways: For the TEM analysis, one determines the relative number of particles with the same size based on defined bin sizes, and only relatively few individual NPs are accounted for. In contrast, SAXS analysis is performed in a larger volume of sample and substantially more NPs are considered for the size evaluation. Additionally, the size retrieved from TEM is often number- or surface-weighted, whereas it is volume-weighted for SAXS, that is, SAXS is more sensitive to the contribution of larger NP sizes. This explains why SAXS analysis leads to an estimated diameter slightly larger than for TEM analysis in this study. Nevertheless, due to the good agreement of the results obtained by both analysis techniques in the present

study, we do not distinguish in the following between the two methods when referring to the average particle size and size distribution.

The analysis shows that the average particle sizes range from roughly 2 to 5 nm (Figure 1). In addition, the carbon support of each investigated catalyst is relatively homogeneously decorated by Pt particles; in particular, the TKK 19.4 wt.% Pt/C sample. The limited particle agglomeration on the carbon support of this catalysts is also reflected by the very narrow size distribution with a standard deviation of only 0.4 nm in the TEM analysis. As expected, it can be clearly seen that at increased Pt loadings, the carbon support is more densely covered with Pt particles and agglomeration increases. Characteristically in the TEM micrographs of the HISPEC 60 wt.% and 70 wt.% Pt/C samples, some darker spots are seen that most likely are related to the slightly agglomerated Pt particles and the size distribution exhibits a clearly discernable tail towards larger sizes (also the size distribution of the TKK 50.6 wt.% Pt/C sample displays such a feature).

In Figure 2, SEM-EDS cross-sections of pristine GDEs prepared from three representative Pt/C catalysts are shown. The general structure of the GDEs consisting of a porous GDL covered by a carbon MPL and the respective Pt/C catalyst layer is clearly discernable. While the MPL's thickness is measured constantly to be around 20 μm, the
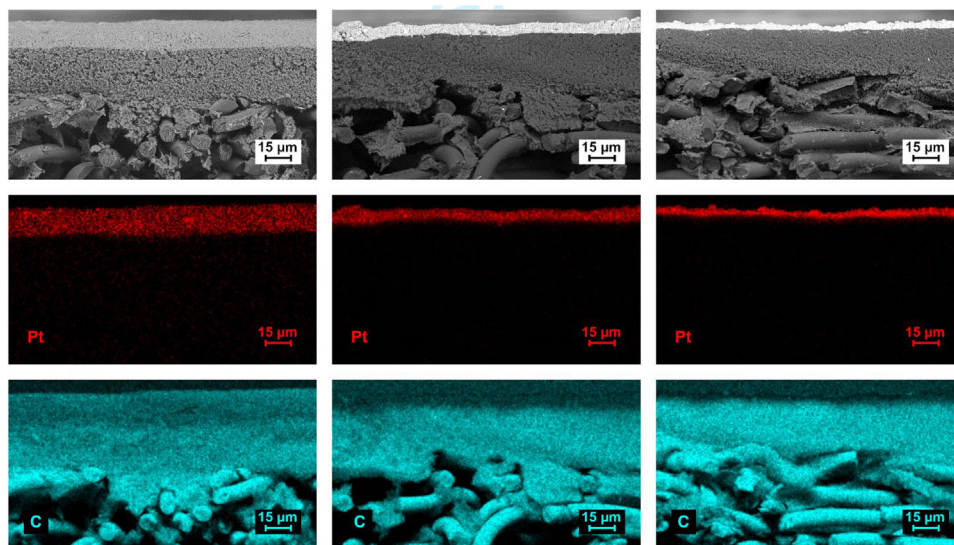
6   **Electrochemical Science Advances**

RESEARCH ARTICLE
doi.org/10.1002/elsa.202100190

Chemistry
Europe
European Chemical
Societies Publishing

FIGURE 2   Comparison of SEM-EDS cross-sections of three GDEs prepared with different Pt/C catalysts. (Left) HISPEC 20 wt.%, (middle) TKK 46 wt.%, and (right) HISPEC 70 wt.%. The SEM micrographs were recorded with the BSE detector. Due to the different metal loading on the carbon support in the Pt/C catalysts, the fixed Pt loading on the GDL (208 ug_{Pt}/cm^2) leads to different thicknesses of the catalyst film

thickness of the Pt/C catalyst layer varies with the Pt loading on the carbon support (Pt to carbon ratio) of the respective catalyst. At low Pt loading (20 wt.%), the catalyst film is about 16 ± 1 µm, whereas it is less than 5 µm on average at very high Pt loading (70 wt.%). In other words, higher Pt loadings (Pt to carbon ratio) of the Pt/C catalyst lead to substantially denser (thinner) catalyst layers. Furthermore, the SEM micrographs imply that under current conditions, the vacuum filtration method of the Pt/C catalysts with high Pt wt.% leads to less homogeneous catalyst films on the GDL.

In previous work of our and other groups, the TKK 46 wt.% Pt/C sample was used as a benchmark or reference catalyst.[14,16,17,30] Therefore, in the following, we discuss the GDE measurements with this catalyst. In the upper part of Figure 3, representative CVs of the TKK 46 wt.% Pt/C samples recorded in the two setups are compared. In both cases, the typical "electrochemical features" of a Pt/C catalyst are depicted. In the low potential region of the CVs (0.05–0.35 V_{RHE}), both hydrogen adsorption (negative scanning direction) and desorption (positive scanning direction) are visible, typically referred to as H_{upd} peaks. However, the H_{upd} peaks in the CV of the GDE measurements differ from the ones in the RDE, which are typical for measurements in aqueous perchloric acid electrolyte. In particular, the CV recorded in the GDE setup, the "second" peak at around 0.25 V_{RHE} is less pronounced, and the hydrogen evolution reaction (HER) starts earlier, around 0.07 V_{RHE}. In contrast to these differences, the adjacent potential region between 0.35 V_{RHE} and 0.60 V_{RHE}, the double layer region defined by capacitive currents from
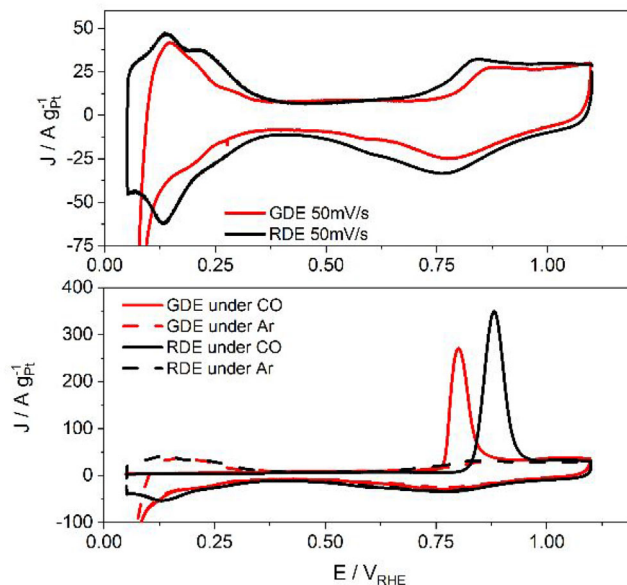

FIGURE 3   In the upper graph, representative examples of CVs of the same TKK 46 wt.% Pt/C catalyst recorded in an inert (Ar purging) atmosphere are shown, whereas in the lower graph, representative CO stripping measurements of the same catalyst are shown. The CVs are normalized to the Pt loading on the electrode to take account of the different films thicknesses. The measurements recorded in the RDE setup are represented by a black line, while the measurements recorded in the GDE setup are represented by a red line. The scan rate was 50 mV/s for both GDE and RDE

charging and discharging the interphase, displays identical double layer capacities in both setups. Finally, in the potential region of Pt oxidation and reduction (0.60–1.10 V_{RHE}),

the Pt oxidation and reduction peaks in the CV recorded with the GDE setup are shifted toward higher potentials. These observed differences are most likely a consequence of the different local ion environments, that is, an aqueous electrolyte and a membrane electrolyte environment. In the GDE setup, the catalyst is surrounded by a solid Nafion electrolyte, whereas it is surrounded by a liquid aqueous electrolyte in the RDE setup. The earlier onset of the HER in the GDE setup might be related to the reduced local partial pressure of hydrogen. Furthermore, the reference electrode in the GDE setup is in aqueous electrolyte, while the measured catalyst is not. This might lead to slight shifts in referenced and "experienced" potentials, which is known to substantially influence the determination of the intrinsic ORR activity.[29]

The different reaction environments manifest itself also in the CO stripping measurements that are typically used to determine the electrochemically active Pt surface area,[31] see lower graph in Figure 3. The CO oxidation peaks recorded in both setups are clearly shifted against each other. Interestingly, in the GDE setup, the CO stripping peak appears at lower potentials than in the RDE setup (ca. 0.8 vs. 0.9 V_{RHE}). Thus, the shift is more pronounced and in opposite direction as compared to the potential difference in hydrogen evolution or oxide formation observed in the CVs recorded in Ar atmosphere. It should be pointed out that this shift is not related to an incomplete CO monolayer formation, as can be seen from the absence of H_{upd} features in the forward going CO stripping scan. Therefore, it can be argued that the shift in the CO stripping peak is related to a reduced anion blocking in the GDE membrane-catalyst environment.[32] Interestingly, the peak position observed in the CO stripping curve recorded in the GDE setup is similar to the one observed in an MEA measurement by Harzer et al.,[33] although it needs to be stressed out that a direct comparison is difficult due to the different catalyst and different experimental parameters such as scan rate and temperature. In addition, the CO stripping shows a smaller ECSA for the catalyst layer in the GDE setup compared with the RDE setup, which is consistent with the observation in the H_{upd} region, that is, the overall peak area in the H_{upd} region in GDE measurement is smaller than the one from RDE measurement.

To investigate this effect systematically, in Figure 4, the ECSA values obtained from the CO stripping measurements are compared for the different Pt/C catalysts measured in both setups. The ECSA is plotted versus their "theoretical" ECSA, which is calculated from the TEM size histograms assuming that the Pt NPs are perfect, free-standing spheres, that is, no Pt surface area is blocked by the carbon support. The ECSA values of some Pt/C samples can also be compared to previous measurements.[34] The diag-
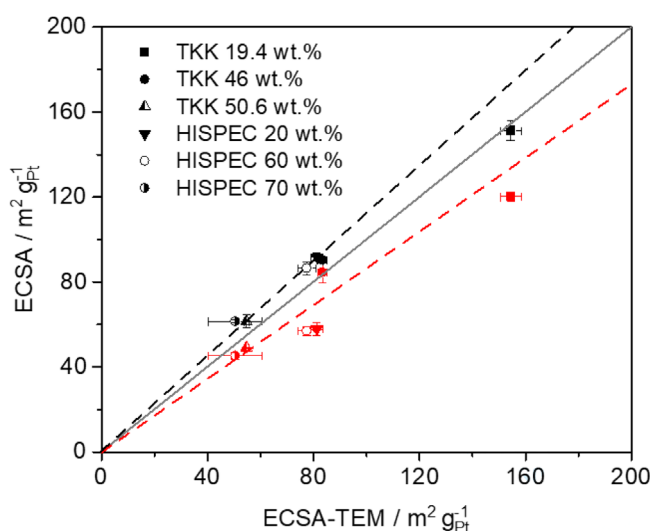

FIGURE 4 Comparison of ECSA values obtained from RDE (black dots) and GDE (red dots) measurements with the ECSA calculated from the Pt particle distribution shown in the TEM micrographs, indicated as ECSA-TEM. The ECSA-TEM values were calculated based on 200–400 randomly distributed Pt particles in the TEM micrographs of each catalyst. The given error with respect to the ECSA-TEM is the standard error of the counted Pt particles in TEM micrographs, while the given error from measured ECSA values is the standard deviation of at least three independent measurements of each catalyst

onal line in Figure 4 indicates where measured and "theoretical" ECSA values are equal. It is seen that there is in general a good agreement between the measured ECSAs and the expected ECSA based on the particle size distribution. However, as a general trend the ECSA values determined in the GDE setup are lower than the ones obtained in the RDE measurements. This general trend is visualized in Figure 4 by fitting linear trendlines to the data points. The maximum difference in ECSA from RDE and GDE is approximately 20%. This systematic difference could be the result of different factors. First, it may be that during the vacuum filtration some Pt got lost, resulting in a smaller CO-oxidation current when normalized to the assumed catalyst loading. Second, Nafion which needs to be added to the catalyst ink preparation for the GDE, might block some active sites. Nafion is known to partially block the active surface area of the active catalyst phase and, thus, reduces the ECSA.[35] For the RDE measurements, no Nafion was used as its only function is to glue the catalyst film to the GC.[36]

In Figure 5, the electrochemical response of the Pt/C benchmark catalyst in O_2 saturated atmosphere is presented from measurements by both setups, that is, the RDE and the GDE setup. The goal of an RDE characterization is to determine the intrinsic kinetic ORR activity of a catalyst. Such task is challenging as in the past even the results of
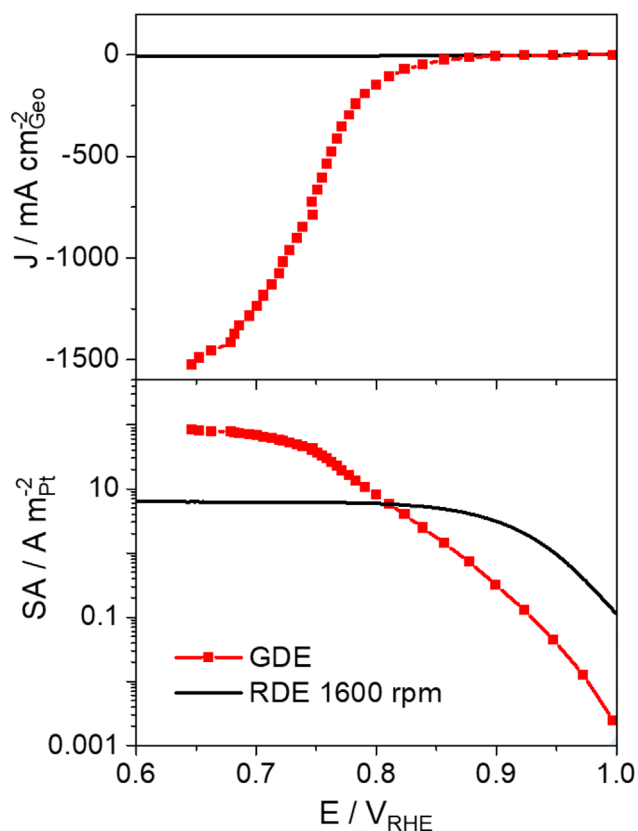
FIGURE 5   Comparison of the ORR performance of TKK 46 wt.% Pt/C measured in a GDE (red) and RDE setup (black). Upper graph, excerpt of the geometric ORR current densities

FIGURE 6   Comparison of the corresponding potential loss at a current of 5 A/m_{Pt}^2 from RDE and GDE. The potential loss is a result of subtraction between the averaged corresponding potential in RDE and GDE. The bar from TKK 50.6 wt.% Pt/C with the dashed edge is a measurement result with cleaning the catalyst surface in Ar saturated electrolyte in RDE, while the same catalyst with a bar of solid edge is a measurement result companied with an optimized cleaning procedure (O_2 saturated electrolyte). The given error is the standard deviation for the difference in averaged corresponding potential at the current of 5 A/m_{Pt}^2 between RDE and GDE

relatively "simple" Pt/C catalysts had been varying by one order of magnitude.[9] As a result, benchmarks, such as polycrystalline Pt, have been introduced and several works on measurement procedures and best practices have been published.[8,25,26,29,31,37] The basic assumption is that procedures and conditions can be defined where all catalysts exhibit their maximum performance. Focusing first on the measurement limitations of the RDE setup, it is seen that the maximum ORR current density which can be reached (at 1600 rpm) is around 6 mA/cm$^2_{Geo.}$ The broad current plateau indicates that in a wide potential region, the ORR is limited by mass transport through the hydrodynamic layer at the electrode interface.[38] By contrast, in the GDE setup, a current density up to 1400 mA/cm$^2_{Geo}$ can be reached in the same potential region because oxygen gas can directly diffuse through the GDL to the catalyst layer. Thus, the maximum current density achieved in the present study is comparable to the ones reported from MEA tests, for example, at 0.7 V, 1500 mA/cm^2 could be reached in H$_2$-O$_2$ MEA tests using a Pt-Co/C catalyst.[39,40] A GDE setup is, thus, particularly apt at investigating catalysts with higher current densities and lower potentials, which reflect more realistic conditions that are closer to the operational win-
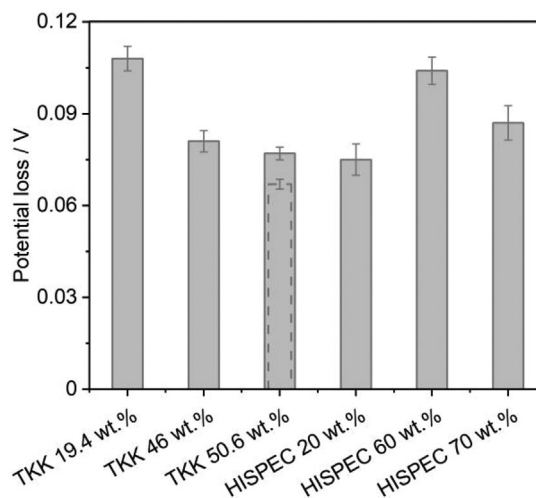
dow of a fuel cell. It should be mentioned though, that the maximum current density reached in the GDE setup varied up to 50% between the different samples, highlighting the influence of the catalyst layer on the obtained results.

To further compare the results, the current densities were normalized to the ECSA derived from the CO stripping measurements, thus, avoiding any influence from uncertainties in catalyst loading. This specific ORR activity is shown as a Tafel plot in Figure 5. The Tafel plot shows that the potential region with kinetic behavior, that is, linear Tafel slope is substantially larger in a GDE setup as compared to a RDE measurement; it stretches from around 1 V$_{RHE}$ down to roughly 0.75 V$_{RHE}$ whereas the kinetically controlled potential region ends at around 0.90 V$_{RHE}$, in a RDE measurement. However, it is also seen, that the SA obtained in the low-current regime (above 0.80 V$_{RHE}$) of RDE measurements is substantially higher than the one measured in the GDE setup. This difference in SA was observed for all six investigated Pt/C catalysts and is summarized in Figure 6. Comparing the performance of the different Pt/C catalysts with a standardized procedure at a fixed current density of 5 A/m_{Pt}^2, a potential shift in the range of 0.067 V$_{RHE}$ and 0.108 V$_{RHE}$ is observed between the two approaches which constitutes a substantial difference of around one order in magnitude.

To investigate the reason for this significant reduction in SA measured in the GDE setup, we applied a steady-state

9   **Electrochemical Science Advances**   RESEARCH ARTICLE
doi.org/10.1002/elsa.202100190

**Chemistry
Europe**
European Chemical
Societies Publishing

protocol using an RDE. Supporting information Figure S3 shows that by applying a steady-state protocol in an RDE measurement, the SA at 0.9 V_{RHE} drops down to a similar SA, that is, 0.4 A/m$^2_{Pt}$ as was measured in the GDE setup at the same potential. This indicates that the substantial differences in determined specific ORR activities in the GDE setup are at least partially caused by the steady-state protocol used for GDE measurements. In the GDE measurements, we started the measurements at 1.00 V_{RHE} and went stepwise more negative to 0.10 V_{RHE}, where each step took 1 min. Thus, at each potential, we can assume steady-state conditions. In contrast, in the dynamic potential cycling typically used for RDE measurements, no steady-state condition is reached, leading to an apparent higher activity. The effect is also well-known from RDE measurements, where a profound influence of the scan rate on the ORR activity is reported and a hysteresis in activity between positive and negative sweeps is observed.[9,41] Furthermore, in a RDE measurement, the kinetic current density is obtained after correcting for mass transport limitations.[42] All these arguments point toward that in the intrinsic ORR activities derived from RDE measurements might overestimate the performance in a fuel cell, where steady-state conditions are applied. The GDE setup, by comparison, is not particularly designed to investigate catalysts under dynamic conditions and applying a similar protocol using a GDE setup is not feasible. Any uncompensated resistance (iR drop) leads not only to a shift in potential but also to a current-dependent change in the scan rate. Potentiostatic or galvanostatic measurements by comparison can be corrected for the iR drop in a straightforward manner but face the challenge of a more or less pronounced time dependence in the recorded current or potential. Hence in the current work, we choose to average the currents recorded in a set time interval, see section 2. Instead of investigating the catalysts properties at 0.90 V_{RHE}, the focus is set to lower voltages with higher current densities, which reflects more realistic conditions, that is, in the range between 0.70 V_{RHE} and 0.80 V_{RHE}. This range equals the operational window for a real fuel cell and is, thus, especially important. For the GDE measurements, we adopted a procedure of Yarlagadda et al.[43] to prepare Pt/C films on top of a GDL using the same Pt loading and a standardized ink composition for all Pt/C catalysts. Furthermore, the same automized testing protocol has been applied, see section 2. The activity results then can be compared at either a fixed potential or at fixed current density. Apart from these systematic differences between RDE and GDE measurements which should lead to a constant shift in activity between all catalysts, the different measurement results of the 50.6 wt.% catalyst in Figure 6 indicate that an automized and standardized procedure might not always be suitable to ensure that each catalyst exhibits its opti-
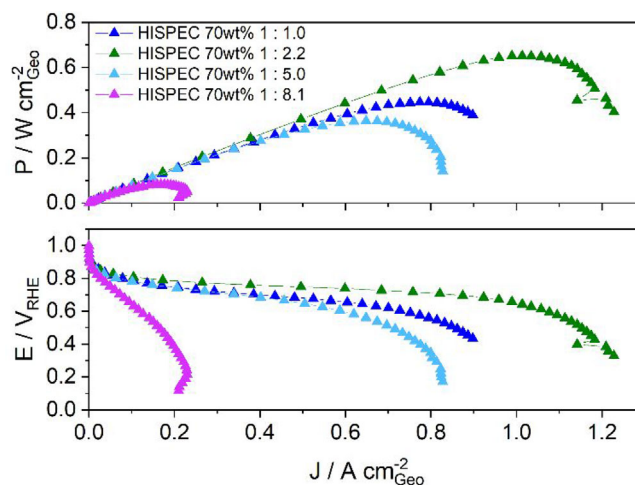

FIGURE 7   Comparison of different carbon to Nafion ratios (C:N) of HISPEC 70 wt.%. The power density of HISPEC 70 wt.% strongly depends on the amount of Nafion added to the ink. The standard procedure suggests a C:N ratio of 1:1. However, measurements made with the GDE setup show higher power density for a C:N ratio of 1:2.2. By adding significantly more Nafion, the power density drops down

mal, intrinsic performance in a GDE measurement. For example, an improved cleaning procedure in oxygen might improve the performance (in the specific case shown here, in the RDE measurements) while for other catalysts it might lead to slight degradation, for example, in case of small particles. Furthermore, the SEM-EDS cross-sections demonstrate substantially different thicknesses of the Pt/C catalyst films depending on the Pt loading on the carbon support.

Furthermore, in comparative RDE measurements, typically the same ink composition is used for all Pt/C catalysts without optimization for a specific catalyst. However, a fixed carbon to Nafion (C:N) mass ratio, might not be the best recipe for all the different catalysts. The different Pt loadings on the carbon support, the different Pt particle size distributions as well as different carbon supports might require specific ink compositions for every single catalyst to optimize the performance in the GDE setup; knowledge that is commonly known for MEA measurements and is part of the optimization of fuel cell catalyst layers.[44]

To investigate this hypothesis, we analyzed the specific ORR activity (SA) of a moderately performing catalyst, that is, the HISPEC 70 wt.% at different C:N mass ratios. As demonstrated in Figure 7, the conventional ink recipe (C:N = 1:1) does not lead to the best performance of the HISPEC 70 wt.% catalyst. The obtained maximum power density strongly depends on the C:N ratio in the ink (Figure 7). By changing the C:N ratio, the maximum power density can be almost doubled from about 0.4 to about 0.7 W/cm^2. A

standardized ink recipe, therefore, leads to an "underperformance" of certain catalysts. For a meaningful comparison of different catalysts in a GDE, it is, therefore, important to consider optimizing the ink composition for every single catalyst.

To demonstrate this conclusion even further, and to analyze which characteristics are crucial for a good performance of a specific Pt/C catalyst, we also analyzed the influence of the Pt to Nafion (Pt:N) ratio of this specific catalyst by introducing additional carbon support in the catalyst ink. In the plot in Figure 8, it is demonstrated that at 0.9 V_{RHE}, the ORR performance increases with increasing C:N ratio. With regards to the Pt:N ratio, it seems that the ORR performance increases with increasing ratio as well. However, this behavior changes as soon as higher current densities are reached. At 0.8 V_{RHE}, the highest ORR current density was reached with a Pt:N ratio of 1 instead of a ratio more than 2 at 0.9 V_{RHE}. Furthermore, it is shown that at this Pt:N ratio, the C:N ratio does not have a substantial influence on the current density anymore. This trend gets even more pronounced at 0.7 V_{RHE}. The highest current density for the HISPEC 70 wt.% catalyst were obtained with a Pt:N ratio of 1 (by adding carbon support to the ink) *and* a C:N ratio of 1.

4 | CONCLUSIONS

In the presented work, the ORR performance of six commercial Pt/C catalysts is compared in a GDE setup. As benchmark, the same catalysts are compared in RDE measurements according to standardized procedures that are assumed to showcase the *intrinsic* ORR activity of the respective catalysts. The results are summarized in Table 1. The work clearly demonstrates the challenges but also the strengths of the GDE approach. In the last 10 years, several RDE studies demonstrated the importance of the film quality for obtaining the intrinsic ORR activity of a catalyst, research work that is still ongoing.[45] At the same time, the popularity of the RDE approach is at least partially owed to its simplicity and the availability of all required instruments. The presented GDE measurements indicate that the influence of the film quality on the obtained results in this approach is at least equally important as in the RDE approach. However, to find broad application, a simple and straight-forward film preparation method should be applied, such as the vacuum filtration technique, that only requires standard equipment that is available in most research laboratories and leads to reproducible results in film quality. Most likely, as for the RDE approach, further work on establishing standardized procedures and the use of benchmarks will be essential to obtain meaningful results.
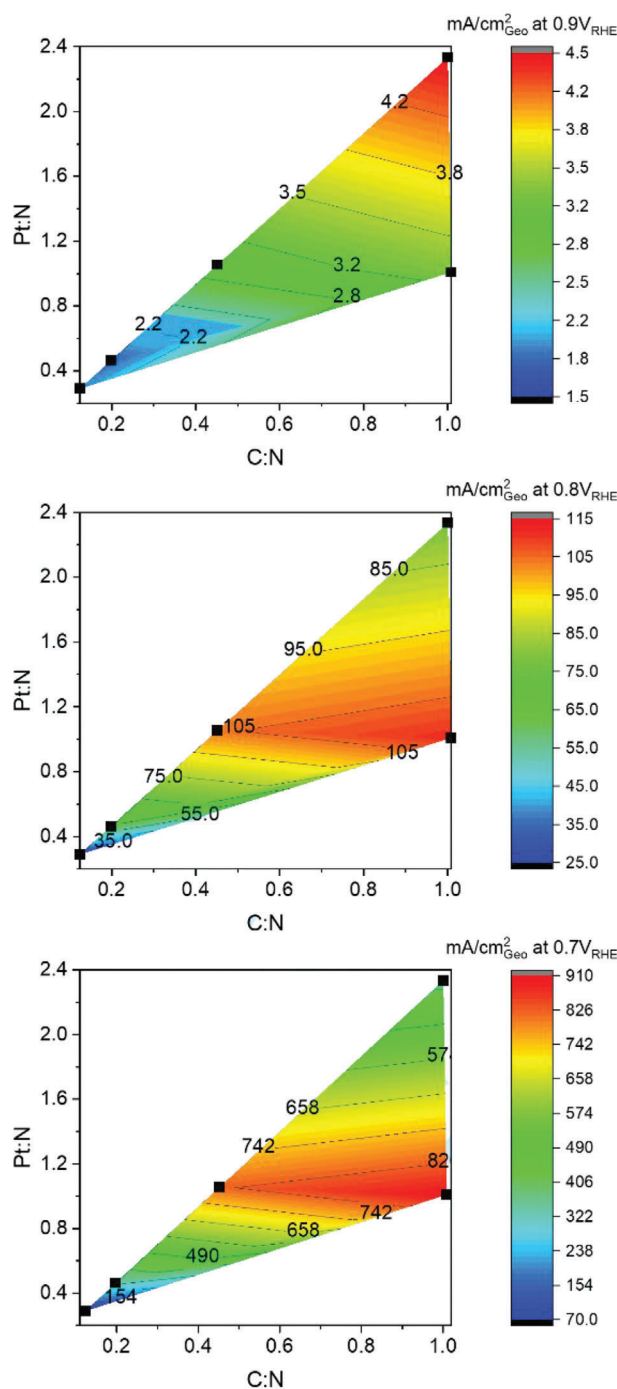

FIGURE 8 Comparison of the influence of Pt:N and C:N ratios on ORR activities of HISPEC 70 wt.% at 0.9 V_{RHE}, 0.8 V_{RHE}, and 0.7 V_{RHE}. At 0.9 VRHE, both Pt:N and C:N ratio determine the obtained current density of HISPEC 70wt.%. A high Pt:N ratio and a C:N ratio around 1 gave the highest current densities. However, at lower voltages the Pt:N ratio becomes the key ratio. There is a clear trend toward a Pt:N ratio of 1. The ORR activities are averaged values of three measurements. The black squares indicate the calculated C:N and Pt:N ratios of all analyzed catalyst films based on which the contour plots are made

4
— 11

Electrochemical Science Advances

— RESEARCH ARTICLE
doi.org/10.1002/elsa.202100190

TABLE 1 Summary of the RDE and GDE results. The font in red from TKK 50.6 wt.% is the result with potential cycling in O_2 for catalyst surface cleaning

Catalyst	Pt NP size (nm) TEM	Pt NP size (nm) SAXS	Theoretical M ECSA (m^2/g_{Pt}) Based on TEM	ECSA (m^2/g_{Pt}) RDE	ECSA (m^2/g_{Pt}) GDE	MA (A/g_{Pt}) RDE (0.9 V)	MA (A/g_{Pt}) GDE (0.9 V)	MA (A/g_{Pt}) GDE (0.8 V)	SA (A/m_P) RDE (0.9 $V_{Pos.}$)	SA (A/m_P) RDE (0.9 $V_{Neg.}$)	SA (A/m_P) GDE (0.9 V)	SA (A/m_P) GDE (0.8 V)
TKK 19.4 wt.%	1.6 ± 0.4	1.9 ± 0.3	175	151.3 ± 7.5	120.1 ± 2.3	163.4 ± 59	12.2 ± 0.6	330	3.37 ± 0.49	1.08 ± 0.39	0.1	2.75
TKK 46 wt.%	2.9 ± 0.8	2.8 ± 0.5	96.5	90.3 ± 1.1	84.6 ± 5	108.4 ± 11.8	26.7 ± 0.9	660	5.84 ± 0.99	1.20 ± 0.13	0.3	7.8
TKK 50.6 wt.%	4.7 ± 1.1	5.4 ± 1.7	59.5	61.4 ± 3.3	49 ± 0.2	55.3 ± 7.4	16.8 ± 0.4	364	3.18 ± 0.28 / 4.20 ± 0.36	0.90 ± 0.11 / 1.68 ± 0.14	0.3	7.43
HISPEC 20 wt.%	2.9 ± 0.8	3.3 ± 1.1	96.5	91.8 ± 2.1	57.8 ± 3.2	175.3 ± 8.3	19.4 ± 2.7	517	5.64 ± 1.21	1.91 ± 0.09	0.3	8.95
HISPEC 60 wt.%	2.9 ± 1	3.3 ± 0.8	96.5	86.5 ± 3.4	57 ± 2	174.7 ± 17.3	9.7 ± 0.1	280	5.69 ± 1.14	2.02 ± 0.20	0.2	5
HISPEC 70 wt.%	3.5 ± 1.5	4 ± 0.8	79.8	61.5 ± 0.7	45.3 ± 1.6	113.2 ± 40	21.4 ± 0.7	379	6.77 ± 2.00	1.84 ± 0.65	0.5	8.4

On the other hand, the results clearly demonstrate the potential of the GDE approach to bridge RDE and MEA measurements, thus, helping to commercialize new ORR catalysts. Most importantly, the GDE approach allows focusing on relevant current densities that are inaccessible in RDE measurements. Moreover, the optimization of characteristics, such as the ink recipe or the applied catalyst loading on the GDL for each individual catalyst, is feasible in a much simpler manner than in elaborate MEA testing. Therefore, the GDE approach has the clear potential to reach similar popularity as the RDE approach.

ACKNOWLEDGMENTS
This work was supported by the Swiss National Science Foundation (SNSF) via the project No. 200021_184742. Jia Du acknowledges funding from the China Scholarship Council (CSC). Jonathan Quinson acknowledges the European Union's Horizon 2020 research and innovation program under the Marie Skłodowska-Curie grant agreement No. 840523 (CoSolCat). S. B. Simonsen and L. Theil Kuhn, Technical University of Denmark, are thanked for access to TEM. The Niels Bohr Institute, University of Copenhagen, for access to SAXS equipment and in particular J. J. K. Kirkensgaard.

CONFLICT OF INTERESTS
The authors declare no conflict of interest.

ORCID
Etienne Berner https://orcid.org/0000-0002-4902-2687
Gustav K.H. Wiberg https://orcid.org/0000-0003-1884-604X
Matthias Arenz https://orcid.org/0000-0001-9765-4315

REFERENCES
1. T. Yoshida, K. Kojima, *Electrochem. Soc. Interface* **2015**, *24*, 45–49.
2. F. R. Nikkuni, B. Vion-Dury, L. Dubau, F. Maillard, E. A. Ticianelli, M. Chatenet, *Appl. Catal. B Environ.* **2014**, *156–157*, 301–306.
3. D. J. Myers, A. Jeremy Kropf, E. C. Wegener, H. Mistry, N. Kariuki, J. Park, *J. Electrochem. Soc.* **2021**, *168*, 044510.
4. H. A. Baroody, E. Kjeang, *J. Electrochem. Soc.* **2021**, *168*, 044524.
5. D. J. S. Sandbeck, N. M. Secher, M. Inaba, J. Quinson, J. E. Sørensen, J. Kibsgaard, A. Zana, F. Bizzotto, F. D. Speck, M. T. Y. Paul, A. Dworzak, C. Dosche, M. Oezaslan, I. Chorkendorff, M. Arenz, S. Cherevko, *J. Electrochem. Soc.* **2020**, *167*, 164501.
6. O. Gröger, H. A. Gasteiger, J.-P. Suchsland, [J. Electrochem. Soc., 162, A2605 (2015)]. *J. Electrochem. Soc.* **2016**, *163*, X3–X3.
7. B. Han, C. E. Carlton, A. Kongkanand, R. S. Kukreja, B. R. Theobald, L. Gan, R. O'Malley, P. Strasser, F. T. Wagner, Y. Shao-Horn, *Energy Environ. Sci.* **2015**, *8*, 258–266.
8. K. Shinozaki, J. W. Zack, R. M. Richards, B. S. Pivovar, S. S. Kocha, *J. Electrochem. Soc.* **2015**, *162*, F1114. https://doi.org/10.1149/2.1071509jes.

12 **Electrochemical Science Advances**

RESEARCH ARTICLE
doi.org/10.1002/elsa.202100190

Chemistry
Europe
European Chemical
Societies Publishing

9. H.A. Gasteiger, S. S. Kocha, B. Sompalli, F. T. Wagner, *Appl. Catal. B* **2005**, *56*, 9–35. https://doi.org/10.1016/j.apcatb.2004.06.021.

10. H. A. Gasteiger, J. E. Panels, S. G. Yan, *J. Power Sources* **2004**, *127*, 162–171.

11. D. Siegmund, S. Metz, V. Peinecke, T. E. Warner, C. Cremers, A. Grevé, T. Smolinka, D. Segets, U. P. Apfel, *JACS Au* **2021**, *1*, 527–535.

12. T. Yoshizumi, H. Kubo, M. Okumura, *SAE Int*. **2021**. https://doi.org/10.4271/2021-01-0740.

13. G. K. H. Wiberg, M. Fleige, M. Arenz, *Rev. Sci. Instrum.* **2015**, *86*. https://doi.org/10.1063/1.4908169

14. M. Inaba, A. W. Jensen, G. W. Sievers, M. Escudero-Escribano, A. Zana, M. Arenz, *Energy Environ. Sci.* **2018**, *11*. http://doi.org/10.1039/C8EE00019K

15. C. Zalitis, A. Kucernak, X. Lin, J. Sharman, *ACS Catal.* **2020**, *10*, 4361–4376.

16. C. M. Zalitis, D. Kramer, A. R. Kucernak, *Phys. Chem. Chem. Phys.* **2013**. https://doi.org/10.1039/c3cp44431g.

17. L. Pan, S. Ott, F. Dionigi, P. Strasser, *Curr. Opin. Electrochem.* **2019**, *18*, 61–71.

18. K. Ehelebe, D. Seeberger, M. T. Y. Paul, S. Thiele, K. J. J. Mayrhofer, S. Cherevko, *J. Electrochem. Soc.* **2019**, *166*, F1259–F1268.

19. B. A. Pinaud, A. Bonakdarpour, L. Daniel, J. Sharman, D. P. Wilkinson, *J. Electrochem. Soc.* **2017**. https://doi.org/10.1149/2.0891704jes.

20. S. Alinejad, M. Inaba, J. Schröder, J. Du, J. Quinson, A. Zana, M. Arenz, *J. Phys. Energy* **2020**, *2*, 024003.

21. J. Schröder, V. A. Mints, A. Bornet, E. Berner, M. Fathi Tovini, J. Quinson, G. K. H. Wiberg, F. Bizzotto, H. A. El-Sayed, M. Arenz, *JACS Au* **2021**, *1*, 247–251.

22. J. Schröder, J. Quinson, J. K. Mathiesen, J. J. K. Kirkensgaard, S. Alinejad, V. A. Mints, K. M. ∅. Jensen, M. Arenz, *J. Electrochem. Soc.* **2020**, *167*, 134515.

23. K. Ehelebe, N. Schmitt, G. Sievers, A. W. Jensen, A. Hrnjić, P. C. Jiménez, P. Kaiser, M. Geuß, Y.-P. Ku, P. Jovanovič, K. J. J. Mayrhofer, B. Etzold, N. Hodnik, M. Escudero-Escribano, M. Arenz, S. Cherevko, *ACS Energy Lett.* **2022**, *7*, 816–826.

24. M. Inaba, J. Quinson, J. R. Bucher, M. Arenz, *J. Vis. Exp.* **2018**, *133*, e57105.

25. S.S. Kocha, K. Shinozaki, J. W. Zack, D. J. Myers, N. N. Kariuki, T. Nowicki, V. Stamenkovic, Y. Kang, D. Li, D. Papageorgopoulos, *Electrocatalysis* **2017**, *8*, 366–374.

26. M. Inaba, J. Quinson, M. Arenz, *J. Power Sources* **2017**, *353*, 19–27.

27. J. Du, J. Quinson, D. Zhang, F. Bizzotto, A. Zana, M. Arenz, *ACS Catal.* **11**, 820–828.

28. J. Du, J. Quinson, A. Zana, M. Arenz, *ACS Catal.* **11**, 7584–7594.

29. K. J. J. Mayrhofer, D.Strmcnik, B.B.Blizanac, V.Stamenkovic, M.Arenz, N.M.Markovic, *Electrochim. Acta* **2008**, *53*, 3181–3188.

30. G. K. H. Wiberg, M. Fleige, M. Arenz, *Rev. Sci. Instrum.* **2015**, *86*.

31. M. Inaba, J. Quinson, J. R. Bucher, M. Arenz, *J. Vis. Exp.* **2018**, *2018*, 57105.

32. D. Zhang, J. Du, J. Quinson, M. Arenz, *ChemRxiv. Prepr.* **2021**. http://doi.org/10.33774/chemrxiv-2021-j5vb5.

33. G. S. Harzer, J. N. Schwämmlein, A. M. Damjanović, S. Ghosh, H. A. Gasteiger, *J. Electrochem. Soc.* **2018**, *165*, F3118–F3131.

34. M. Nesselberger, S. Ashton, J. C. Meier, I. Katsounaros, K. J. Mayrhofer, M. Arenz, *J. Am. Chem. Soc.* **2011**, *133*, 17428–1733.

35. K. Kodama, A. Shinohara, N. Hasegawa, K. Shinozaki, R. Jinnouchi, T. Suzuki, T. Hatanaka, Y. Morimoto, *J. Electrochem. Soc.* **2014**, *161*, F649–F652.

36. I. Takahashi, S. S. Kocha, *J. Power Sources* **2010**, *195*, 6312–6322.

37. D. Voiry, M. Chhowalla, Y. Gogotsi, N. A. Kotov, Y. Li, R. M. Penner, R. E. Schaak, P. S. Weiss, *ACS Nano* **2018**, *12*, 9635–9638.

38. A. J. Bard, L. R. Faulkner, *Electrochemical Methods: Fundamentals and Applications*. Wiley-VCH Verlag, Germany**1980**.

39. X. Tian, X. F. Lu, B. Y. Xia, X. W. Lou (David), . *Joule* **2020**, *4*, 45–68.

40. L. Chong, J. Wen, J. Kubal, F. G. Sen, J. Zou, J. Greeley, M. Chan, H. Barkholtz, W. Ding, D. J. Liu, *Science (80-.).* **2018**, *362*, 1276–1281.

41. U. A. Paulus, T. J. Schmidt, H. A. Gasteiger, R. J. Behm, *Res. gate* **2014**, *495*, 134–145.

42. N. M. Markovíc, P. N. Ross, *Surf. Sci. Rep.* **2002**, *45*, 117–229.

43. V. Yarlagadda, S. E. McKinney, C. L. Keary, L. Thompson, B. Zulevi, A. Kongkanand, *J. Electrochem. Soc.* **2017**, *164*, F845–F849.

44. T. Yoshizumi, H. Kubo, M. Okumura, in *SAE Technical Paper* **2021**.https://doi.org/10.4271/2021-01-0740.

45. M. Inaba, Y. Kamitaka, K. Kodama, *J. Electroanal. Chem.* **2021**, *886*, 115115.

SUPPORTING INFORMATION

Additional supporting information may be found in the online version of the article at the publisher's website.